Response to Referee #2

Dear Referee,

We sincerely appreciate your careful and constructive review of our manuscript. We are grateful for the time and effort you invested in evaluating our work. Your comments have been valuable in helping us improve both the clarity and robustness of the analysis.

We appreciate your summary of the manuscript and your recognition that the overall structure and presentation are clear. We acknowledge your concerns regarding aspects of the analysis that required further clarification. Accordingly, we have carefully addressed each of your comments in detail. The revised manuscript will include:

- Effect of background buoyant forcing in S_l and S_v regardless of aerosol regimes.
- An expanded statistical analysis in the Supplement, including uncertainty quantification and sensitivity tests of the cloud detection thresholds, to better support the N_d - S (S_c, S_l, S_v) relationship.
- A more explicit treatment of the energetic contribution of W_s in the calculation of LWC at cloud base.

We believe that these revisions adequately address your concerns and improve the manuscript to a level suitable for publication.

General comments:
The paper presents a new method that employs the energy budget analysis framework to estimate the amount of supersaturation at warm cloud base by assuming the saturated parcel ascent as reversible adiabatic process with conserved isobaric enthalpy. The authors partition the supersaturation of the cloud (S_c) into vapor-phase (S_v) and liquid-phase (S_l) supersaturations to derive magnitudes of S_c, S_v, and S_l in the context of the energy balance defined by the first law of thermodynamics. This method is complemented by a closure analysis conducted using airborne observations of warm cumulus clouds from the ACRIDICON-CHUVA campaign. The analysis demonstrates how droplet number concentration (N_d) scales with S_v and agrees within the uncertainty range of CCN(S_v) spectra measured below cloud base prior to cloud observations.

Overall, the manuscript is well written and easy to follow. However, some analyses require further clarification. It is recommended that the manuscript be reconsidered after a major revision.

Specific Comments:

1. In section 3.1, please clarify the impact of background buoyant forcing on the estimated values of S_l and S_v using this framework regardless of aerosol regimes. In other words, how do uncertainty in S_l and S_v scales with increasing background buoyant forcing in any given environment?

A: We thank the referee for this important comment.

Background buoyant forcing primarily affects the dynamical evolution of the cloud base parcel, particularly the updraft velocity (w) and the associated cooling rate during ascent. Stronger buoyancy leads to faster adiabatic cooling and enhances the S_v generated along the parcel trajectory at cloud bases (Khain and Pinsky, 2018; Twomey, 1959). However, in the present study, S_l and S_v are not calculated based on the updraft velocity or the aerosol regime. Instead, they are diagnosed from the local thermodynamic state at cloud base and defined as the fractional contributions from the total latent heat release during condensational growth (Q), $\Delta U/Q$ and W_s/Q, respectively. As a result, background buoyant forcing does not directly impose a systematic shift in the relative partitioning between S_l and S_v. For a given thermodynamic state (T, p, LWC), the total energy Q is constrained by the enthalpy change ($dH = Q$), and the partitioning depends primarily on the balance between internal energy change and expansion work. The influence of buoyant forcing is therefore implicit, acting through its influence on the observed cloud base properties.

The figures below show the observed relationships between w, S_v, and S_l for the analysed flights. Since w is dynamically associated with parcel buoyancy, stronger updraft velocities produce increased spread and variability in S_v and S_l, particularly in updraft-limited (CCN-rich) regimes (e.g., during flight AC07), whereas in CCN-limited regimes the sensitivity to w is weaker (e.g., during flight AC19). Thus, the buoyant forcing primarily modulates the pathway to the cloud-base thermodynamic state rather than the thermodynamic constraint governing the energy partitioning applied in this study.

As discussed in Braga et al. (2017), and originally noted by Twomey (1959), although N_d is expected to increase with w in an idealized framework, in situ measurements exhibit substantial scatter due to turbulence. Individual cloud parcels ascend as turbulent eddies with locally varying w, and their subsequent mixing within the cloud introduces a large stochastic component to the observed relationship between w and microphysical properties. As a result, the correlation between w and quantities such as N_d and S_v, is often weak, even though the underlying physical dependence remains valid.

Regarding uncertainty, increasing background buoyant forcing tends to enhance variability in cloud base measurements due to stronger vertical gradients in temperature, water vapour, vertical velocity, and droplet concentrations, as well as enhanced turbulence and sampling heterogeneity. This can lead to increased variability in LWC, T, and p, which are the key measurement inputs to the energy budget. However, the uncertainty in S_l and S_v does not scale directly with buoyant forcing itself, but rather with the uncertainty in these measured thermodynamic variables. In our analysis, the propagated uncertainties of S_l and S_v are on

average ~9.2% (8.6 - 9.4%) and ~12.6% (12.3 - 13.2%), respectively, and are dominated by uncertainties in LWC, with secondary contributions from temperature and pressure.

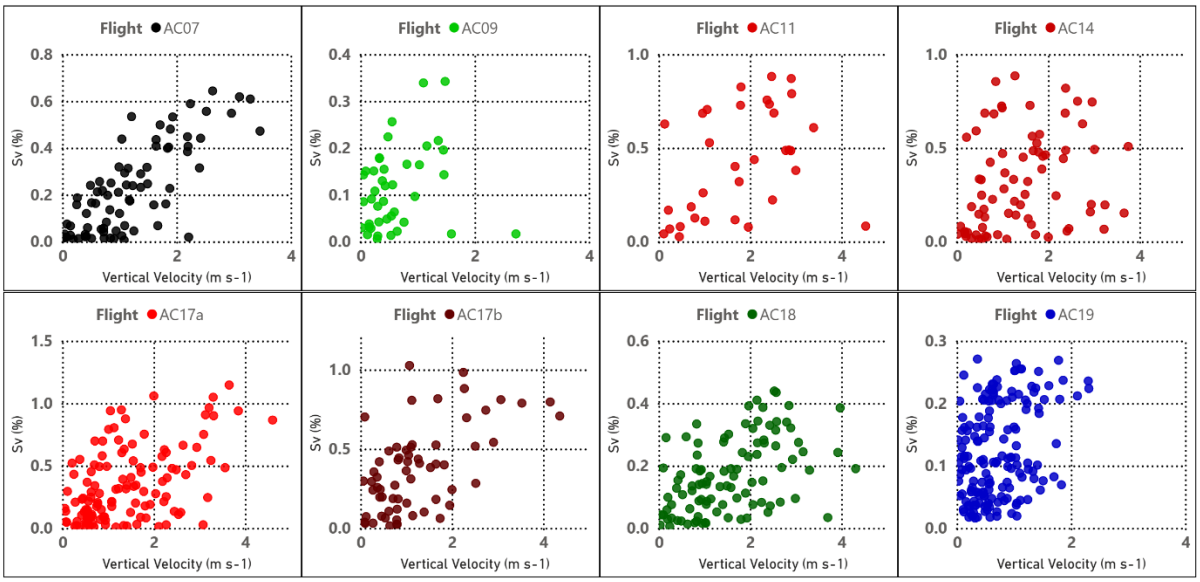

Figure R1. Vertical velocity vs. water vapor supersaturation (S_V). Flight segments are indicated in the legend.

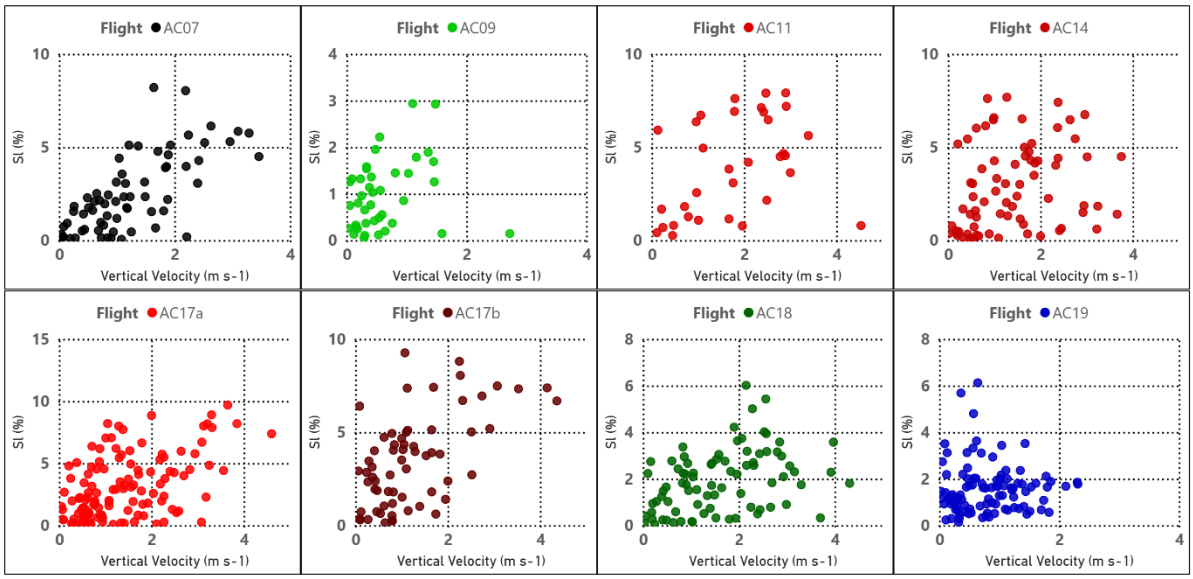

Figure R2. Vertical velocity vs. liquid supersaturation (S_I). Flight segments are indicated in the legend.

2. Cloud passes were considered using a threshold criterion of N_d greater than 20 cm^{-3} at initial stage of cloud formation (Lines 260-265). Since such in-cloud measurement thresholds are currently not standardized in our community, please perform sensitivity analysis on the resulting supersaturations with different threshold criteria defined using a combination of both minimum N_d and/or LWC. Additionally, please verify whether such definitions have any significant impact on the correlation coefficients discussed with power-law fits in Figure 4, S10, and S11. Include the analysis in the supporting information document.

A: Thanks for this comment.

In our previous manuscript (Braga et al., 2017), we had performed cloud base closure analysis using CCP-CDP and CAS-DPOL probes' data from the ACRIDICON-CHUVA campaign. Given the higher accuracy of the CCP-CDP probe from this analysis, we used the probe data in the current study. After several discussions with co-authors (CCP-CDP and CAS-DPOL probes' PI) about the suitable threshold for both probes, we agreed to apply the threshold of $N_d > 20$ cm^{-3} and $w > 0$ m s^{-1} for cloud bases of growing convective cumuli in clean and polluted conditions. This threshold prevented the detection of haze particles and cloud elements during the dissipating stage while calculating parameters relevant to cloud formation.

The cloud supersaturations calculated in this study are sensitive to LWC measured by CCP-CDP. The threshold we applied for cloud identification, in practice, corresponds to an LWC > ~ 0.01 g m^{-3}, as shown in the figures below.

To address the reviewer's request, we performed a sensitivity analysis of the derived supersaturation components (S_c, S_l and S_v) using a range of cloud identification criteria based on varying thresholds of N_d and LWC. The results are summarized in Tables S1-S3.

Overall, the analysis shows that:

- The correlation coefficients (R^2) of the power-law fits ($N_d = C \cdot S^k$) are generally insensitive to the choice of threshold and remain comparable to those obtained using the baseline criterion ($N_d > 20$ cm^{-3}).
- For most flight segments, variations in threshold produce only minor changes in the fitted parameters (C and k), which remain within the estimated uncertainty ranges.
- A notable exception occurs for flight AC07 (polluted conditions), where lower N_d (< 20 cm^{-3}) thresholds introduce increased variability and reduce correlation strength, likely due to inclusion of transitional particles.
- In contrast, for the cleanest case (AC19), slightly improved correlations are obtained when including lower N_d values (< 20 cm^{-3}), consistent with relatively reduced CCN and buoyance variability during cloud formation.

These results show that the derived supersaturations and their relationships, assuming the proposed threshold ($N_d > 20$ cm^{-3}), are robust to reasonable variations in cloud identification criteria. The remaining variability is primarily driven by environmental heterogeneity and

turbulence rather than by the threshold definition itself. All sensitivity analyses will be included in the Supporting Information (similar to what is shown at the end of this document).

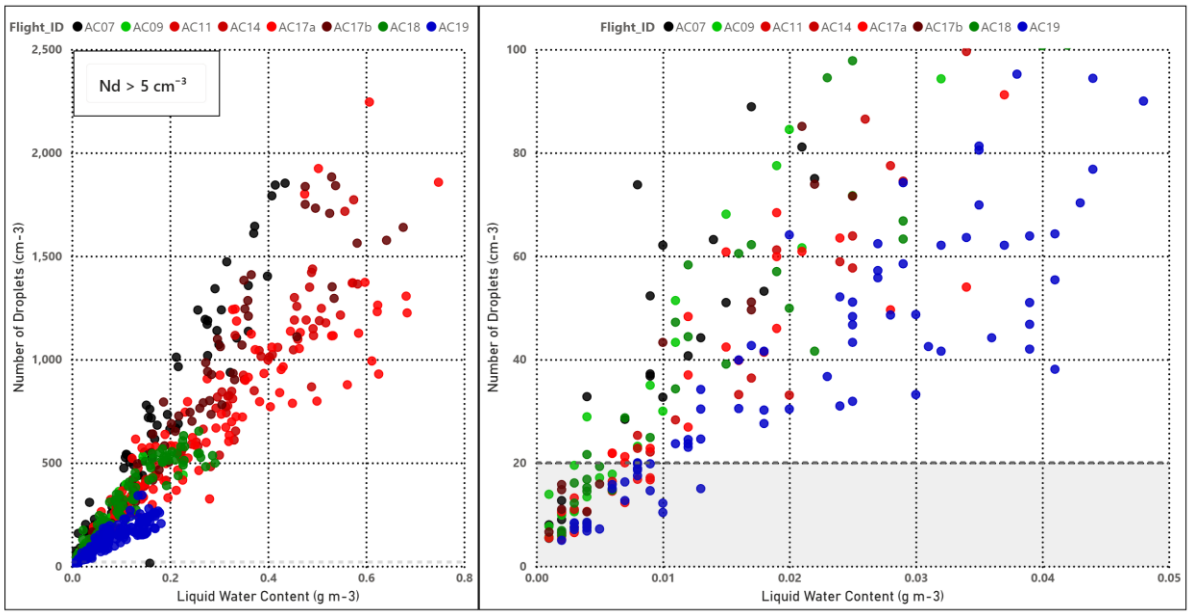

Figure R3. [left] LWC versus N_d for all flight segments. [right] Similar for (N_d < 100 cm^{-3} & LWC < 0.05 g m^{-3}). The threshold N_d = 20 cm^{-3} (dashed line) corresponds approximately to LWC ≳ 0.01 g m^{-3} for most flights' data. The shaded region shows the excluded 1 Hz cloud passes for the adopted criterion (N_d > 20 cm^{-3}).

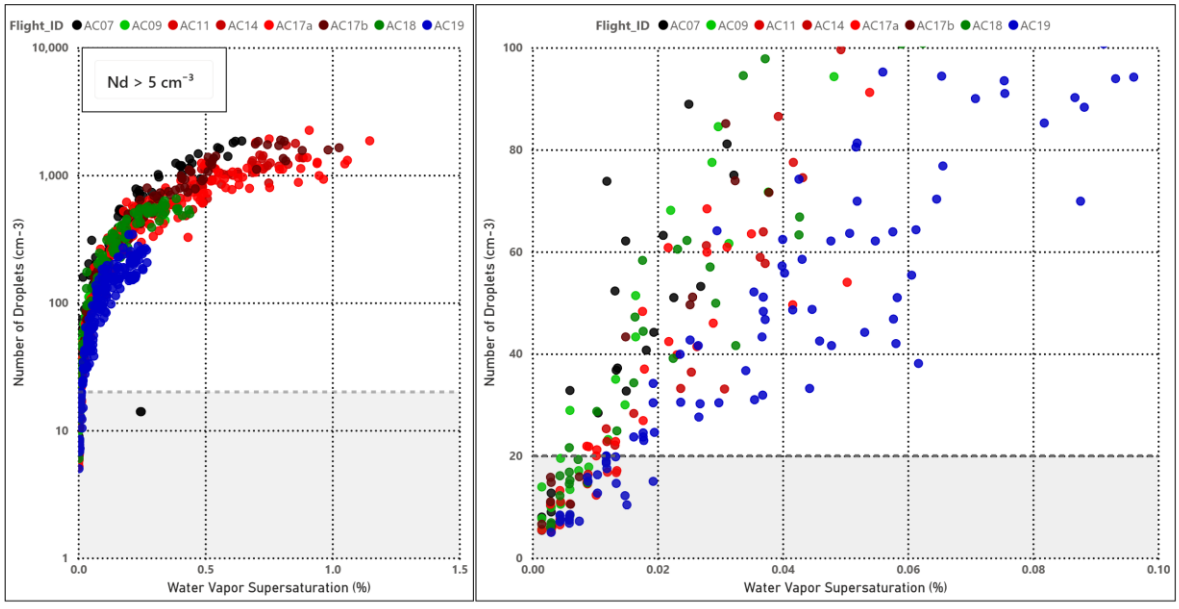

Figure R4. [left] water vapor supersaturation (S_v) vs. N_d for all flight segments (N_d > 5 cm^{-3}). [right] Similar for (N_d < 100 cm^{-3} & Sv < 0.1 %). The shaded region shows the excluded 1 Hz cloud passes for the adopted criterion (N_d > 20 cm^{-3}).

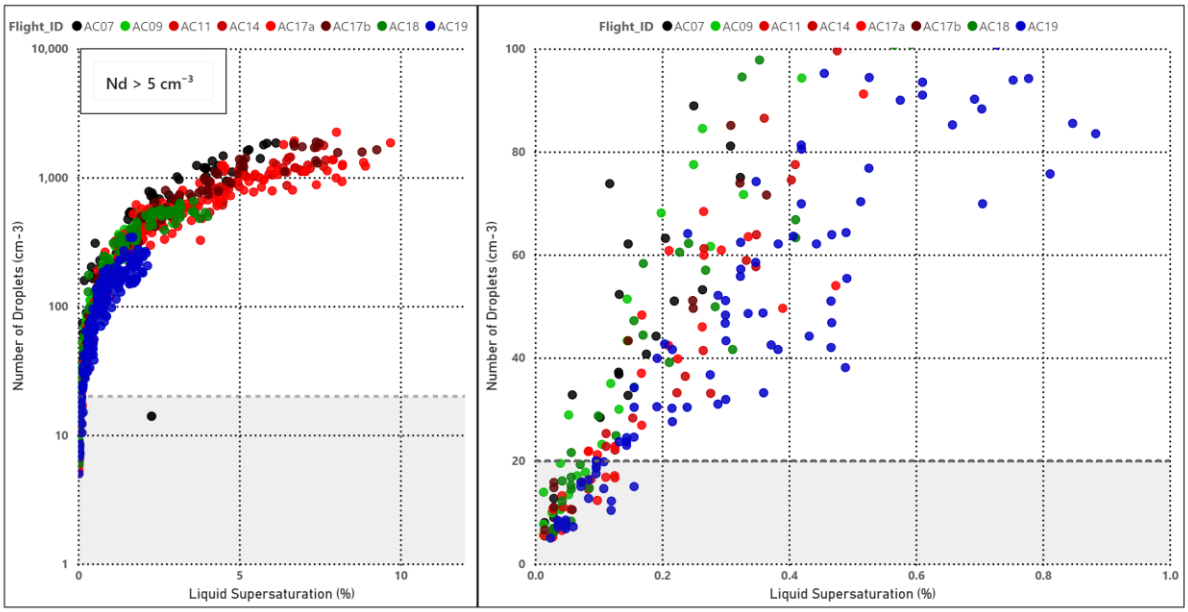

Figure R5. [left] Liquid Supersaturation (Sl) versus N_d for all flight segments ($N_d > 5$ cm^{-3}). [right] Similar for ($N_d < 100$ cm^{-3} & $S_l < 1$ %).

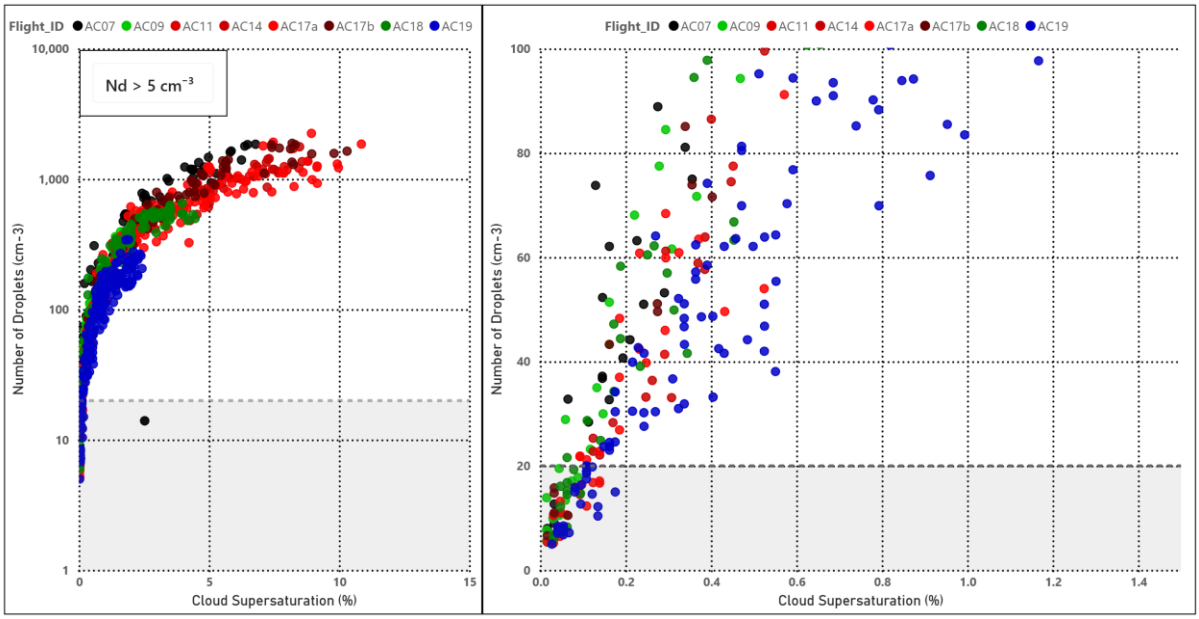

Figure R6. [left] Cloud Supersaturation (S_c) vs. Nd for all flight segments ($N_d > 5$ cm^{-3}). [right] Similar for ($N_d < 100$ cm^{-3} & $S_c < 1.5$ %).

3. The derived correlation coefficients values exhibit inverse correlation with the sample size. Larger sample sizes are associated with lower correlation coefficients and vice versa. Given the extremely limited sample size for this analysis and considering the prior argument, justify whether Nd is well constrained by S_v (Lines 408-409).

A: We agree with the referee that the correlation coefficients are sensitive to sample size and that larger datasets may produce lower R^2 values due to the inclusion of a broader range of atmospheric variability. In our observations, larger samples encompass more heterogeneous conditions in updraft velocity, turbulence intensity, and CCN concentrations, which increases scatter in the N_d-S_v relationship without necessarily invalidating the underlying physical dependence.

We also acknowledge that the present analysis is based on a limited number of cloud-base penetrations from the ACRIDICON-CHUVA campaign. Additional measurements covering a wider range of cloud regimes and environmental conditions would therefore be valuable in future studies to further evaluate the robustness and universality of the fitted power-law parameters.

At the same time, several independent results support the physical consistency of the proposed relationship. The fitted parameters C and k remain relatively stable across the sensitivity tests and threshold selections. More importantly, the N_d (S_v) spectra derived at cloud base agree, within the estimated uncertainties, with the independently measured CCN(S_v) spectra below cloud base (as described in the reply for referee #1).

We have revised the manuscript to clarify these limitations and to avoid overstating the statistical strength of the relationship. The results should therefore be interpreted as evidence supporting the proposed energetic framework and its consistency with cloud base observations, while recognizing that additional datasets are needed to further strengthen the statistical robustness of the derived power-law relationships.

4. The reported uncertainties of 10% for N and LWC at lines 307-309 are applicable only to the ACRIDICON-CHUVA dataset. These uncertainties can be considered as the best-case scenario for measurement uncertainties, given that the Baumgardner et al., 2017 report the uncertainty range for scattering probes for sizing to be 10%-50% and for concentrations to be 10%-30%. Therefore, to extend the energy balance method to be applicable for other datasets from other field campaigns and to account for the worst-case scenario containing the maximum possible range of energy terms and supersaturations, please consider discussing the uncertainty to be defined as both the best-case and worst-case scenarios.

A: In the reply for referee #1 we described the measurement uncertainties calculations applied for the data set. We wrote the following about that:

"Uncertainties in the meteorological measurements from the BAHAMAS system translate into an estimated average uncertainty of about 0.24% (typically < 1% for 1 Hz data) in the derived RHc when calculating using the Bolton equation. The relative uncertainties of the energy terms were about 10% for Q and ΔU, and 13% for Ws. Propagating these errors yields overall uncertainties of ~10% for Sc and Sl, and ~12% for Sv."

The uncertainties of energy terms and supersaturations are mostly sensitive to the LWC uncertainties. Baumgardner et al., (2017) report that the expected range of uncertainties in LWC and N_d is between 10% - 30%. For LWC uncertainty of 30%, the relative uncertainties of the energy terms are about 29% for Q and ΔU, and 38% for W_s. Propagating these errors yields overall uncertainties of ~28% for S_c and S_l, and ~36% for S_v. The figures below show the average values of these uncertainties for each flight, assuming LWC uncertainties of 10% and 30%.

Higher measurement uncertainties increase the scatter in the power-law relationship N_d-S relationship (shown in Tables S4-S6), as reflected by generally lower R^2 and similar or slightly higher RMSE values. However, the impact is not limited to statistical dispersion. The results show a systematic decrease in both C and k when uncertainties increase, indicating that uncertainty propagation affects not only the precision but also the magnitude of the fitted parameters. Despite these shifts, the power-law relationship remains consistent across thresholds and flights, and the variations in C and k are within the broader uncertainty range of the estimates. This indicates that while increased uncertainties reduce the strength of the statistical fit and slightly bias the parameter values, they do not alter the underlying physical dependence of N_d on S_v.

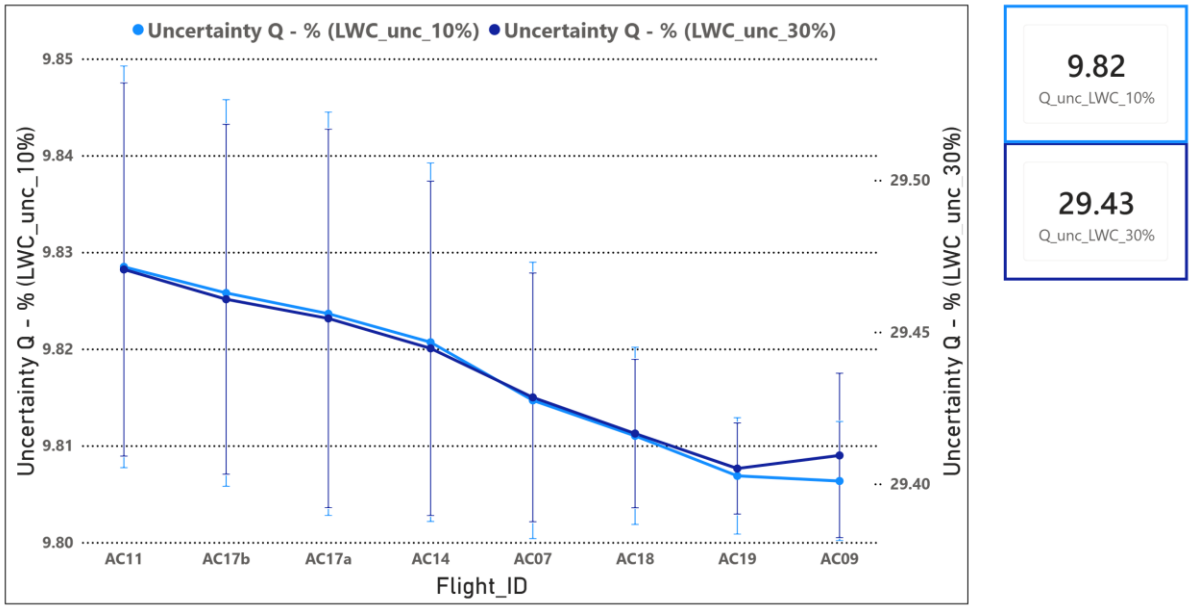

Figure R7. Relative uncertainty (%) of the latent heat term Q for each flight segment, derived from propagated liquid water content (LWC) uncertainties of 10% and 30%. Markers indicate flight-mean values and error bars represent ±1σ variability within each segment. The right panel shows the mean uncertainty across all flights, highlighting the strong sensitivity of Q to LWC uncertainty.

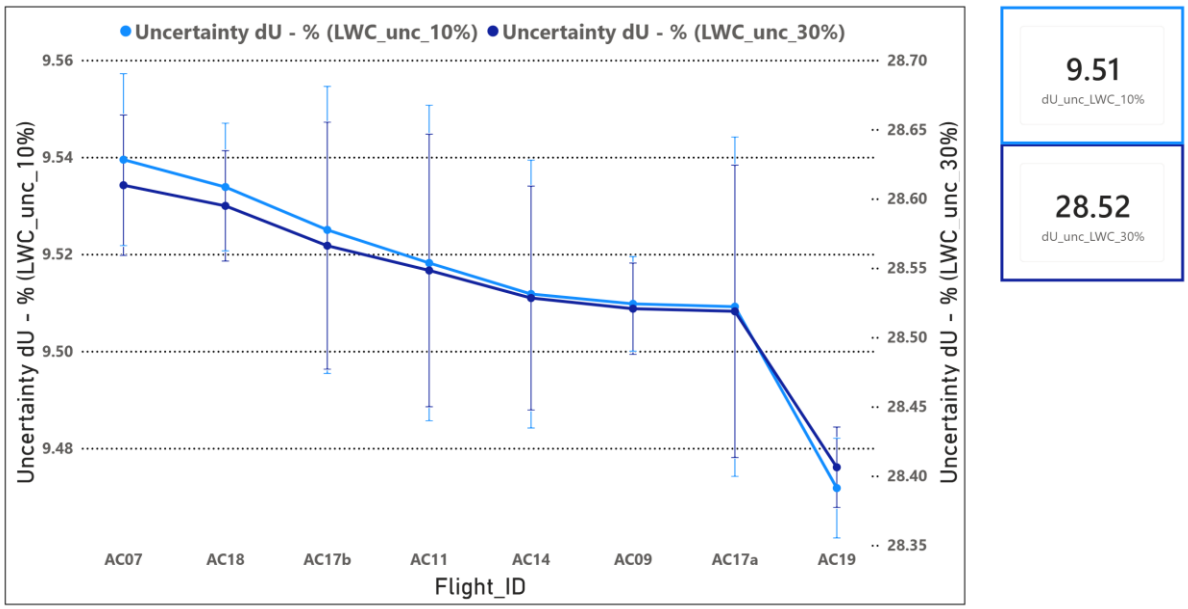

Figure R8. Similar to Figure R7 for the internal energy change ΔU for each flight segment. The right panel summarizes the mean uncertainty across all flights, showing similar sensitivity to LWC as observed for Q.

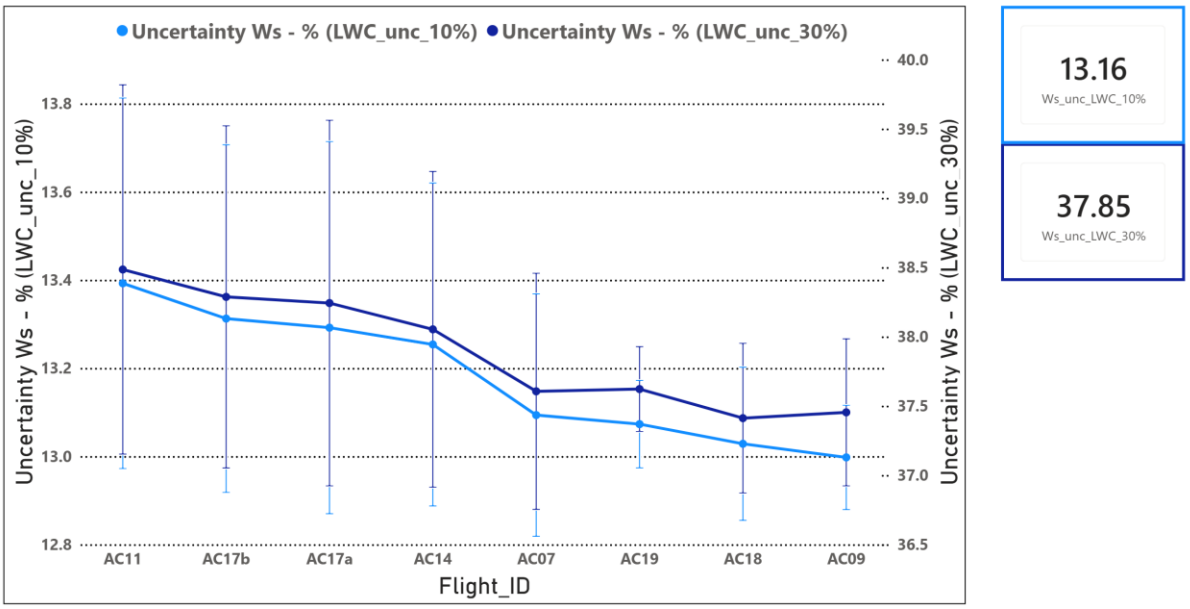

Figure R9. Similar to Figure R7 for the saturation work term W_s for each flight segment. The right panel indicates the mean uncertainty across flights, with larger sensitivity compared to Q and ΔU.

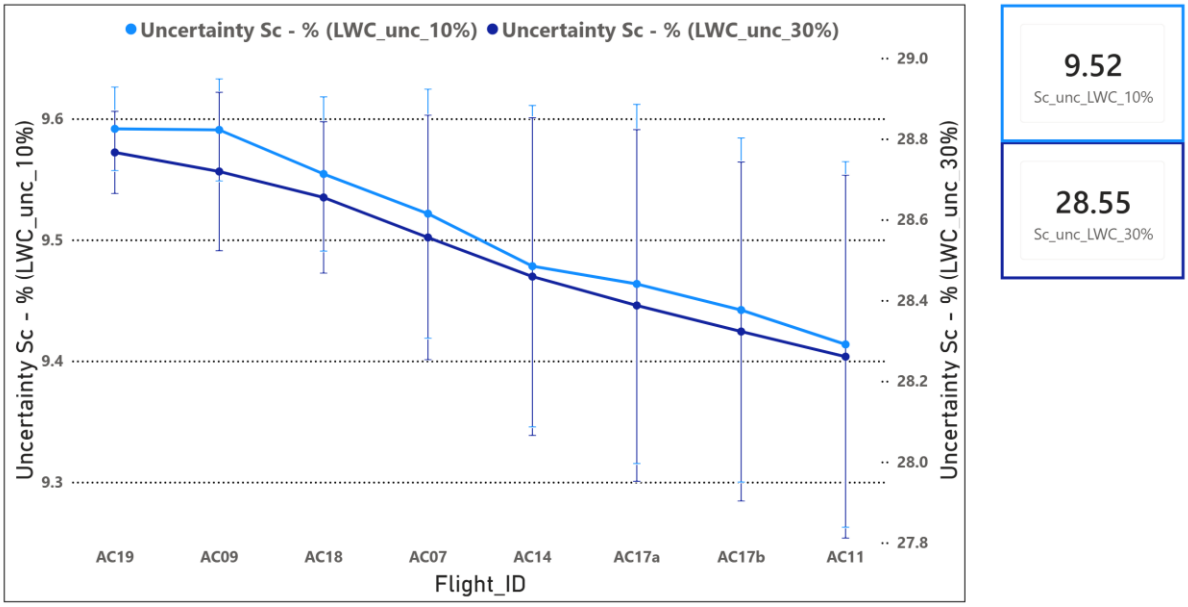

Figure R10. Similar to figure R7 for cloud supersaturation S_c for each flight segment. The right panel presents the mean uncertainty across all flights.

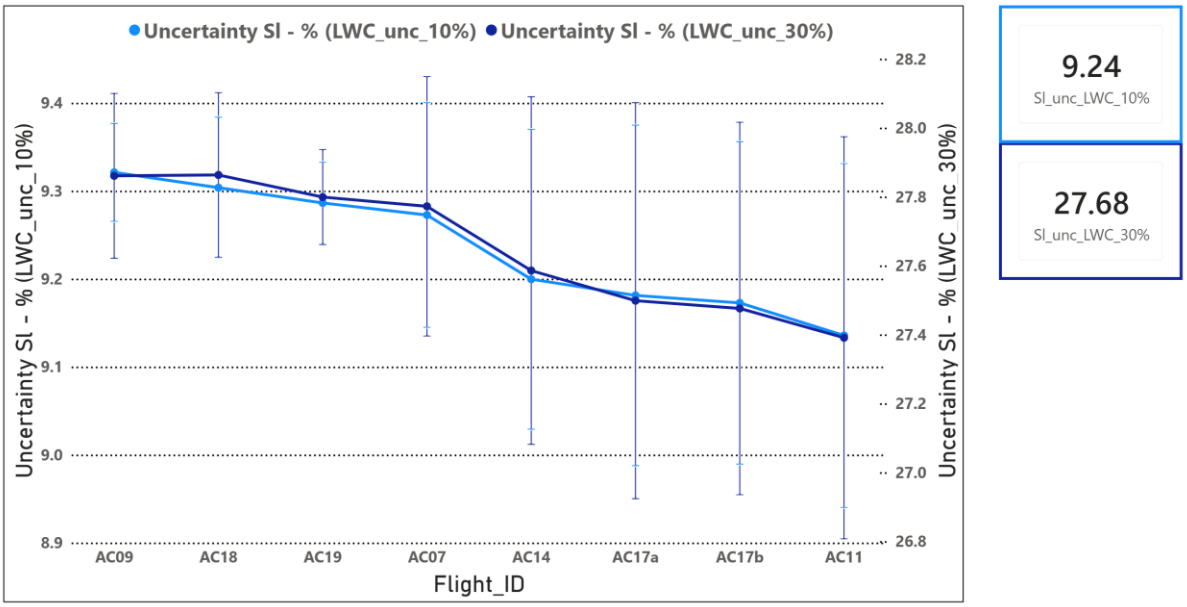

Figure R11. Similar to figure R7 for liquid supersaturation S_l for each flight segment. The right panel presents the mean uncertainty across all flights.

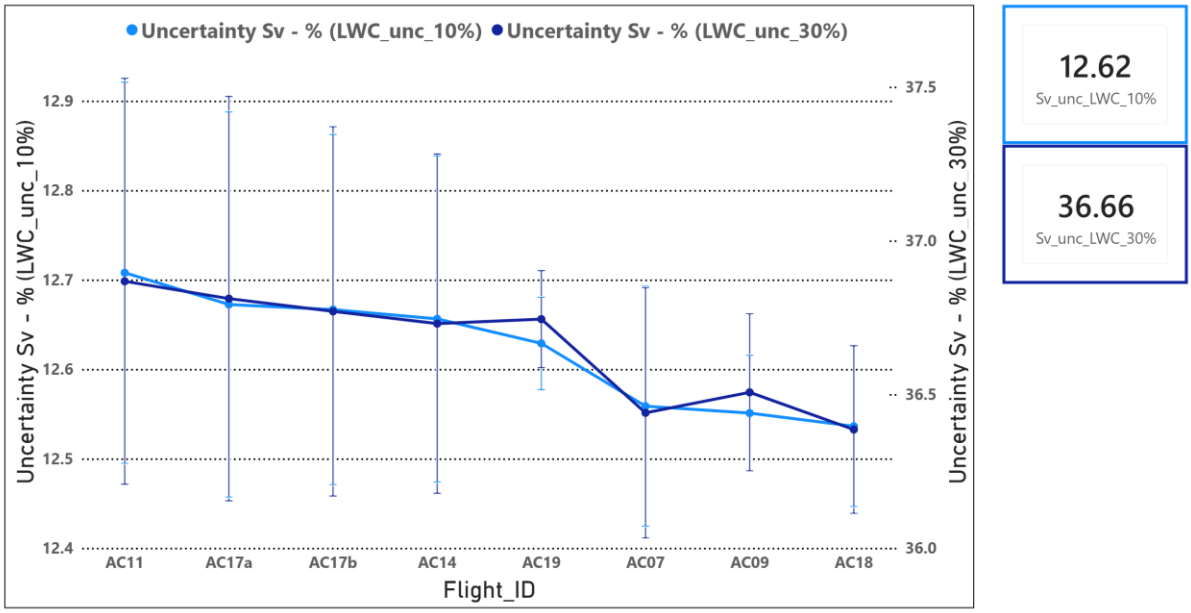

Figure R12. Similar to figure R7 for water vapor supersaturation S_v for each flight segment. The right panel summarizes the mean uncertainty across all flights, indicating higher sensitivity compared to S_c and S_l.

5. Lines 473-474: Please provide the magnitude of overestimation to better highlight the importance of including the energetic cost of vapor expansion during the ascent of the saturated parcel.

A: The figures below quantify the energetic cost of vapor expansion work (W_s) on liquid water content (LWC) estimates at cloud base as a function of adiabatic cooling (ΔT) and initial temperature (T_0) for pressures of 950 hPa and 850 hPa. The inclusion of W_s reduces the LWC by a factor that depends primarily on T_0 and only weakly on ΔT.

At 950 hPa, the fractional reduction in LWC ranges from approximately 4-6% at low temperatures (~ 2-6 °C) to 16-20% at higher temperatures (~ 25-30 °C). At 850 hPa, the reduction is slightly larger, increasing from ~ 5-7% to ~ 18-22% over the same temperature ranges.
At lower pressure, the volumetric LWC is reduced because the dry-air density decreases. At fixed ΔT and T_0, the lower pressure case has a larger saturation mixing ratio (r_s), since it increases as p - $e_s(T_0)$ decreases (see equations below). Therefore, W_s is slightly higher at 850 hPa than at 950 hPa. These factors lead to a larger fractional reduction in LWC when W_s is included.

LWC derivation for the ascending saturated parcel according to the energetic partition:

$$\Delta U = Q - W_s \qquad (1)$$

$$LWC = \rho_{air} \cdot \frac{\Delta U}{L_v} \qquad (2)$$

where:

$$Q = |\Delta H| \quad \therefore \quad L_v \cdot q_l = \left|- c_{\mathrm{p,cloud}} \cdot \Delta T\right| = c_{\mathrm{p,cloud}} \cdot (T_0 - T) \qquad (3)$$

$$q_l = LWC/\rho_{air} \quad (4)$$

$$\rho_{air} = \frac{p - e_s(T_0)}{R_d \cdot T_0} \quad (5)$$

$$W_s = r_{s0} \cdot R_v \cdot T_0 \cdot ln\left(\frac{\propto_{vs}}{\propto_{vs0}}\right) \quad (6)$$

$$r_{s0} = (R_d/R_v) \cdot \frac{e_s(T_0)}{p - e_s(T_0)} \quad (7)$$

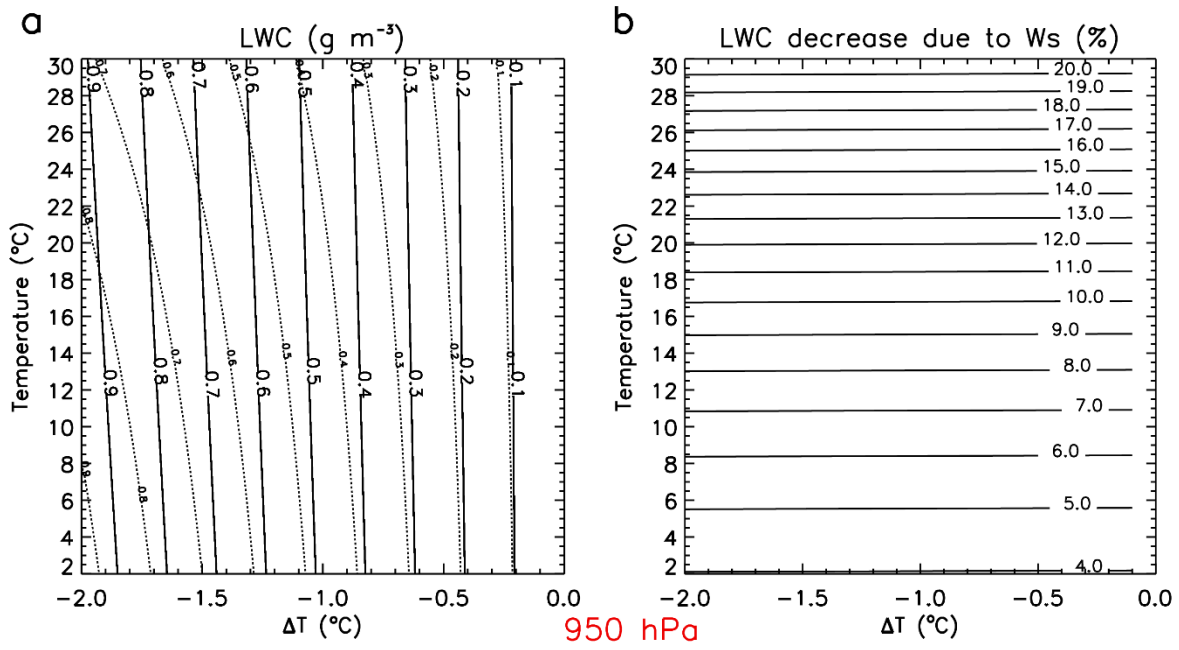

Figure R13. Liquid water content (LWC) and its reduction due to vapor expansion work (W_s) at cloud base for a pressure of 950 hPa, shown as a function of cooling (ΔT) and initial temperature (T_0). (a) LWC (g m^{-3}) calculated assuming all the enthalpy change (Q = dH) contributes to condensational growth of particles (solid contours), with the corresponding LWC including the effect of W_s shown as dotted contours. (b) Fractional decrease in LWC (%) due to the inclusion of W_s.

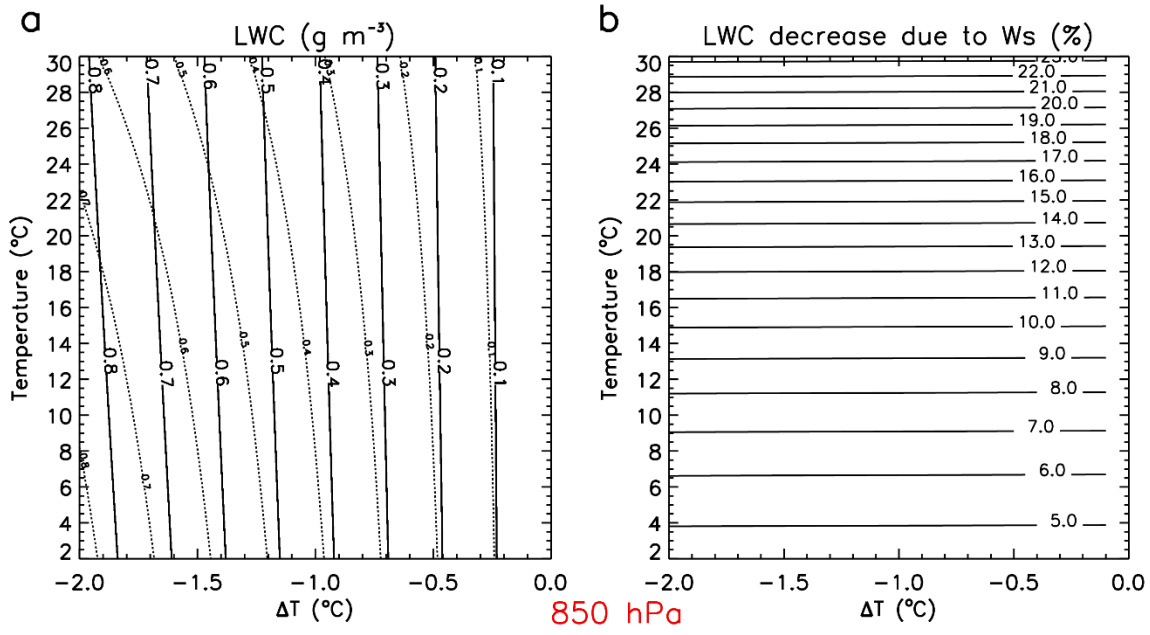

Figure R14. Similar to Figure R13 for 850 hPa.

Technical corrections:

1. The spelling of ‘modeling’ in the manuscript is inconsistent. At Lines 33,36,237, it is spelled as ‘modeling’, whereas at lines 189, 226, 467 it is spelled as ‘modelling’.

A: Ok. Thanks.

2. Figure 3 and 4: Include a description in the figure captions that indicates that the color choices correspond to different aerosol backgrounds in the Amazon region and list the colors with their corresponding regions.

A: Ok. Thanks for this suggestion.

Reference:
Baumgardner, D., and Coauthors, 2017: Cloud Ice Properties: In Situ Measurement Challenges. Meteor. Monogr., 58, 9.1–9.23, https://doi.org/10.1175/AMSMONOGRAPHS-D-16-0011.1
Citation: https://doi.org/10.5194/egusphere-2026-795-RC2

Supporting Information: Sensitivity of the Nd-S relationship to prescribed uncertainties

To quantify the impact of measurement and retrieval uncertainties on the fitted relationship between droplet number concentration and supersaturation, we performed a Monte Carlo uncertainty analysis of the power-law relation:

$$N_d = C \cdot S^k$$

The regression was conducted in log-log space. Uncertainties in both variables were propagated by perturbing the observed values of S (S_c, S_l, and S_v) and N_d assuming Gaussian-distributed errors.

Two uncertainty scenarios were considered for each N_d and S values based on the average uncertainties:

- Best-case scenario: 12.6 % uncertainty in S_v, 9.2 % uncertainty in S_l, 9.5 % uncertainty in S_c, and 10% in N_d.

- Worst-case scenario: 36.6 % uncertainty in S_v, 27.6 % uncertainty in S_l, 28.5 % uncertainty in S_c, and 30% in N_d.

For each case, 5000 Monte Carlo realizations were performed, and the mean and standard deviation of the fitted parameters were calculated (JCGM, 2008).

The conversion of N_d to Standard Temperature and Pressure (STP; p =1013.25 hPa and T = 273.15 K) when comparing with CCN(S_v) spectra measured below cloud bases introduces negligible additional uncertainty relative to the instrumental uncertainty in N_d. For typical cloud base conditions, a temperature uncertainty of 0.5 K contributes approximately 0.17%, while a pressure uncertainty of 3 Pa contributes less than 0.01%. Therefore, the total relative uncertainty in N_{dSTP} remains dominated by the assumed 10% uncertainty in N_d.

References

Campos Braga, R., Rosenfeld, D., Weigel, R., Jurkat, T., Andreae, M. O., Wendisch, M., Pöhlker, M. L., Klimach, T., Pöschl, U., Pöhlker, C., Voigt, C., Mahnke, C., Borrmann, S., Albrecht, R. I., Molleker, S., Vila, D. A., Machado, L. A. T., and Artaxo, P.: Comparing parameterized versus measured microphysical properties of tropical convective cloud bases during the ACRIDICON-CHUVA campaign, Atmos. Chem. Phys., 17, 7365–7386, https://doi.org/10.5194/acp-17-7365-2017, 2017.

Joint Committee for Guides in Metrology: Evaluation of measurement data — Supplement 1 to the "Guide to the expression of uncertainty in measurement" — Propagation of distributions using a Monte Carlo method, Evaluation, JCGM 101:2, 2008.

Khain, A. P. and Pinsky, M.: Physical Processes in Clouds and Cloud Modeling, https://doi.org/10.1017/9781139049481, 2018.

Twomey, S.: The nuclei of natural cloud formation part II: The supersaturation in natural clouds and the variation of cloud droplet concentration, Geofisica Pura e Applicata, 43, 243–249, https://doi.org/10.1007/BF01993560, 1959.

Table S1. Power-law fit parameters for the relationship $N_d = C \cdot S_v^k$ derived from log–log regression. The coefficients $C$and $k$are reported as Monte Carlo means ± 1σ (n = 5000 realizations). The coefficient of determination (R^2) and root-mean-square error (RMSE) are calculated from the nominal fit in logarithmic space. Data are filtered using threshold criteria $N_d > N_{d,\mathrm{th}}$ and $\mathrm{LWC} > \mathrm{LWC_{th}}$. The uncertainties of Nd and Sv assumed in the calculations are 10% and 12.6%, respectively. Columns list: Flight ID, $N_{d,\mathrm{th}}$, $\mathrm{LWC_{th}}$, C, σ C, k, σ k, R^2, RMSE, and sample size (N).

Flight	$N_{d,\mathrm{th}}$	$\mathrm{LWC_{th}}$	C	σC	k	σk	R^2	RMSE	N
AC07	10	0	2017.67	66.2	0.883	0.013	0.783	0.645	81
AC07	10	0.01	2068.73	82.01	0.899	0.02	0.657	0.678	71
AC07	10	0.02	2062.85	100.38	0.896	0.028	0.533	0.698	64
AC07	**20**	**0**	**2414.84**	**82.16**	**0.922**	**0.014**	**0.958**	**0.249**	**77**
AC07	20	0.01	2478.51	92.39	0.939	0.018	0.947	0.234	69
AC07	20	0.02	2441.89	102.81	0.926	0.024	0.943	0.193	62
AC07	30	0	2396.08	82.23	0.917	0.014	0.956	0.25	76
AC07	30	0.01	2478.51	92.39	0.939	0.018	0.947	0.234	69
AC07	30	0.02	2441.89	102.81	0.926	0.024	0.943	0.193	62
AC09	10	0	1347.58	67.91	0.832	0.015	0.956	0.244	48
AC09	10	0.01	1306.68	96.08	0.808	0.029	0.941	0.169	37
AC09	10	0.02	1406.77	132.03	0.845	0.042	0.91	0.173	32
AC09	**20**	**0**	**1349.85**	**85.34**	**0.826**	**0.023**	**0.952**	**0.19**	**41**
AC09	20	0.01	1306.68	96.08	0.808	0.029	0.941	0.169	37
AC09	20	0.02	1406.77	132.03	0.845	0.042	0.91	0.173	32
AC09	30	0	1326.86	93.99	0.815	0.028	0.949	0.167	38
AC09	30	0.01	1306.68	96.08	0.808	0.029	0.941	0.169	37
AC09	30	0.02	1406.77	132.03	0.845	0.042	0.91	0.173	32
AC11	10	0	1575.37	61.52	0.931	0.02	0.99	0.125	35
AC11	10	0.01	1565.84	67.87	0.924	0.028	0.982	0.125	33
AC11	10	0.02	1535.06	66.03	0.9	0.03	0.98	0.118	32
AC11	**20**	**0**	**1565.84**	**67.87**	**0.924**	**0.028**	**0.982**	**0.125**	**33**
AC11	20	0.01	1565.84	67.87	0.924	0.028	0.982	0.125	33
AC11	20	0.02	1535.06	66.03	0.9	0.03	0.98	0.118	32
AC11	30	0	1565.84	67.87	0.924	0.028	0.982	0.125	33
AC11	30	0.01	1565.84	67.87	0.924	0.028	0.982	0.125	33
AC11	30	0.02	1535.06	66.03	0.9	0.03	0.98	0.118	32
AC14	10	0	1595.69	49.67	0.951	0.015	0.979	0.18	74
AC14	10	0.01	1651.26	55.23	0.978	0.018	0.977	0.166	70
AC14	10	0.02	1604.71	54.92	0.948	0.02	0.972	0.153	65
AC14	**20**	**0**	**1643.14**	**52.98**	**0.973**	**0.016**	**0.981**	**0.164**	**73**
AC14	20	0.01	1651.26	55.23	0.978	0.018	0.977	0.166	70
AC14	20	0.02	1604.71	54.92	0.948	0.02	0.972	0.153	65
AC14	30	0	1650.02	54.81	0.977	0.019	0.975	0.167	69
AC14	30	0.01	1650.02	54.81	0.977	0.019	0.975	0.167	69

AC14	30	0.02	1604.71	54.92	0.948	0.02	0.972	0.153	65
AC17a	10	0	1501.55	31.98	0.928	0.009	0.961	0.271	131
AC17a	10	0.01	1460.03	34.89	0.899	0.013	0.934	0.263	117
AC17a	10	0.02	1449.64	37.55	0.891	0.017	0.9	0.267	108
AC17a	**20**	**0**	**1465.85**	**34.06**	**0.903**	**0.012**	**0.947**	**0.26**	**121**
AC17a	20	0.01	1460.03	34.89	0.899	0.013	0.934	0.263	117
AC17a	20	0.02	1449.64	37.55	0.891	0.017	0.9	0.267	108
AC17a	30	0	1449.85	35.18	0.892	0.014	0.931	0.263	116
AC17a	30	0.01	1449.85	35.18	0.892	0.014	0.931	0.263	116
AC17a	30	0.02	1449.64	37.55	0.891	0.017	0.9	0.267	108
AC17b	10	0	1893.74	53.69	0.916	0.013	0.978	0.201	69
AC17b	10	0.01	2002.72	67.55	0.963	0.02	0.973	0.159	63
AC17b	10	0.02	1978.54	68.29	0.95	0.023	0.967	0.16	61
AC17b	**20**	**0**	**1983.55**	**64.99**	**0.954**	**0.019**	**0.975**	**0.161**	**64**
AC17b	20	0.01	2002.72	67.55	0.963	0.02	0.973	0.159	63
AC17b	20	0.02	1978.54	68.29	0.95	0.023	0.967	0.16	61
AC17b	30	0	1983.55	64.99	0.954	0.019	0.975	0.161	64
AC17b	30	0.01	2002.72	67.55	0.963	0.02	0.973	0.159	63
AC17b	30	0.02	1978.54	68.29	0.95	0.023	0.967	0.16	61
AC18	10	0	1470.38	45.75	0.866	0.012	0.961	0.214	106
AC18	10	0.01	1405.33	53.13	0.84	0.017	0.927	0.212	96
AC18	10	0.02	1321.65	58.49	0.8	0.022	0.881	0.211	87
AC18	**20**	**0**	**1417.28**	**51.16**	**0.845**	**0.016**	**0.94**	**0.213**	**99**
AC18	20	0.01	1405.33	53.13	0.84	0.017	0.927	0.212	96
AC18	20	0.02	1321.65	58.49	0.8	0.022	0.881	0.211	87
AC18	30	0	1405.33	53.13	0.84	0.017	0.927	0.212	96
AC18	30	0.01	1405.33	53.13	0.84	0.017	0.927	0.212	96
AC18	30	0.02	1321.65	58.49	0.8	0.022	0.881	0.211	87
AC19	10	0	790.19	25.96	0.855	0.012	0.912	0.247	177
AC19	10	0.01	756.29	28.46	0.833	0.015	0.875	0.244	164
AC19	10	0.02	725.67	33.31	0.811	0.02	0.817	0.243	148
AC19	**20**	**0**	**740.31**	**27.76**	**0.822**	**0.015**	**0.874**	**0.24**	**163**
AC19	20	0.01	740.31	27.76	0.822	0.015	0.874	0.24	163
AC19	20	0.02	725.67	33.31	0.811	0.02	0.817	0.243	148
AC19	30	0	714.42	29.42	0.804	0.017	0.847	0.243	157
AC19	30	0.01	714.42	29.42	0.804	0.017	0.847	0.243	157
AC19	30	0.02	725.67	33.31	0.811	0.02	0.817	0.243	148

Table S2. Power-law fit parameters for the relationship $N_d = C \cdot S_l^k$ derived from log–log regression. The coefficients $C$and $k$are reported as Monte Carlo means ± 1σ (n = 5000 realizations). The coefficient of determination (R^2) and root-mean-square error (RMSE) are calculated from the nominal fit in logarithmic space. Data are filtered using threshold criteria $N_d > N_{d,\mathrm{th}}$ and $\mathrm{LWC} > \mathrm{LWC_{th}}$. The uncertainties of N_d and S_l assumed in the calculations are 10% and 9.2%, respectively. Columns list: Flight ID, $N_{d,\mathrm{th}}$, $\mathrm{LWC_{th}}$, C, σ C, k, σ k, R^2, RMSE, and sample size (N).

Flight	$N_{d,\mathrm{th}}$	$\mathrm{LWC_{th}}$	C	σC	k	σk	R^2	RMSE	N
AC07	10	0	268.66	4	0.895	0.011	0.788	0.638	81
AC07	10	0.01	263.48	4.7	0.919	0.017	0.664	0.671	71
AC07	10	0.02	262.04	6.19	0.926	0.024	0.543	0.691	64
AC07	**20**	**0**	**293.63**	**4.51**	**0.932**	**0.012**	**0.958**	**0.249**	**77**
AC07	20	0.01	288.53	5.22	0.954	0.016	0.948	0.233	69
AC07	20	0.02	290.75	6.53	0.948	0.021	0.942	0.194	62
AC07	30	0	294.76	4.63	0.927	0.012	0.956	0.249	76
AC07	30	0.01	288.53	5.22	0.954	0.016	0.948	0.233	69
AC07	30	0.02	290.75	6.53	0.948	0.021	0.942	0.194	62
AC09	10	0	221.36	4.72	0.838	0.013	0.957	0.243	48
AC09	10	0.01	225.78	4.88	0.821	0.026	0.944	0.166	37
AC09	10	0.02	223.16	5.14	0.866	0.037	0.913	0.169	32
AC09	**20**	**0**	**224.22**	**4.88**	**0.836**	**0.02**	**0.953**	**0.188**	**41**
AC09	20	0.01	225.78	4.88	0.821	0.026	0.944	0.166	37
AC09	20	0.02	223.16	5.14	0.866	0.037	0.913	0.169	32
AC09	30	0	225.51	4.88	0.829	0.024	0.951	0.164	38
AC09	30	0.01	225.78	4.88	0.821	0.026	0.944	0.166	37
AC09	30	0.02	223.16	5.14	0.866	0.037	0.913	0.169	32
AC11	10	0	187.75	5.06	0.953	0.017	0.99	0.121	35
AC11	10	0.01	186.53	6.54	0.959	0.025	0.983	0.12	33
AC11	10	0.02	192.65	7.45	0.936	0.027	0.981	0.114	32
AC11	**20**	**0**	**186.53**	**6.54**	**0.959**	**0.025**	**0.983**	**0.12**	**33**
AC11	20	0.01	186.53	6.54	0.959	0.025	0.983	0.12	33
AC11	20	0.02	192.65	7.45	0.936	0.027	0.981	0.114	32
AC11	30	0	186.53	6.54	0.959	0.025	0.983	0.12	33
AC11	30	0.01	186.53	6.54	0.959	0.025	0.983	0.12	33
AC11	30	0.02	192.65	7.45	0.936	0.027	0.981	0.114	32
AC14	10	0	190.43	3.25	0.969	0.013	0.981	0.173	74
AC14	10	0.01	185.13	3.59	1	0.015	0.979	0.157	70
AC14	10	0.02	190.9	4.37	0.975	0.018	0.974	0.147	65
AC14	**20**	**0**	**186.46**	**3.33**	**0.993**	**0.014**	**0.983**	**0.157**	**73**
AC14	20	0.01	185.13	3.59	1	0.015	0.979	0.157	70
AC14	20	0.02	190.9	4.37	0.975	0.018	0.974	0.147	65
AC14	30	0	185.14	3.78	1	0.016	0.977	0.158	69

AC14	30	0.01	185.14	3.78	1	0.016	0.977	0.158	69
AC14	30	0.02	190.9	4.37	0.975	0.018	0.974	0.147	65
AC17a	10	0	188.32	2.3	0.948	0.008	0.964	0.261	131
AC17a	10	0.01	193.17	2.94	0.929	0.012	0.938	0.254	117
AC17a	10	0.02	192.78	3.79	0.931	0.015	0.907	0.258	108
AC17a	**20**	**0**	**193.22**	**2.72**	**0.928**	**0.01**	**0.951**	**0.251**	**121**
AC17a	20	0.01	193.17	2.94	0.929	0.012	0.938	0.254	117
AC17a	20	0.02	192.78	3.79	0.931	0.015	0.907	0.258	108
AC17a	30	0	194.63	2.99	0.923	0.012	0.935	0.254	116
AC17a	30	0.01	194.63	2.99	0.923	0.012	0.935	0.254	116
AC17a	30	0.02	192.78	3.79	0.931	0.015	0.907	0.258	108
AC17b	10	0	234.08	4.08	0.931	0.011	0.979	0.195	69
AC17b	10	0.01	218.89	5.28	0.991	0.018	0.976	0.15	63
AC17b	10	0.02	221.56	5.91	0.982	0.02	0.97	0.151	61
AC17b	**20**	**0**	**222.25**	**5.02**	**0.979**	**0.017**	**0.977**	**0.153**	**64**
AC17b	20	0.01	218.89	5.28	0.991	0.018	0.976	0.15	63
AC17b	20	0.02	221.56	5.91	0.982	0.02	0.97	0.151	61
AC17b	30	0	222.25	5.02	0.979	0.017	0.977	0.153	64
AC17b	30	0.01	218.89	5.28	0.991	0.018	0.976	0.15	63
AC17b	30	0.02	221.56	5.91	0.982	0.02	0.97	0.151	61
AC18	10	0	208.28	2.6	0.878	0.01	0.962	0.21	106
AC18	10	0.01	210.65	2.84	0.858	0.015	0.93	0.208	96
AC18	10	0.02	215.24	3.39	0.826	0.02	0.885	0.207	87
AC18	**20**	**0**	**210.1**	**2.8**	**0.861**	**0.014**	**0.942**	**0.209**	**99**
AC18	20	0.01	210.65	2.84	0.858	0.015	0.93	0.208	96
AC18	20	0.02	215.24	3.39	0.826	0.02	0.885	0.207	87
AC18	30	0	210.65	2.84	0.858	0.015	0.93	0.208	96
AC18	30	0.01	210.65	2.84	0.858	0.015	0.93	0.208	96
AC18	30	0.02	215.24	3.39	0.826	0.02	0.885	0.207	87
AC19	10	0	133.38	1.43	0.869	0.011	0.914	0.244	177
AC19	10	0.01	133.61	1.42	0.852	0.013	0.878	0.241	164
AC19	10	0.02	133.78	1.42	0.838	0.018	0.82	0.241	148
AC19	**20**	**0**	**133.75**	**1.41**	**0.841**	**0.014**	**0.876**	**0.238**	**163**
AC19	20	0.01	133.75	1.41	0.841	0.014	0.876	0.238	163
AC19	20	0.02	133.78	1.42	0.838	0.018	0.82	0.241	148
AC19	30	0	133.96	1.41	0.825	0.015	0.85	0.24	157
AC19	30	0.01	133.96	1.41	0.825	0.015	0.85	0.24	157
AC19	30	0.02	133.78	1.42	0.838	0.018	0.82	0.241	148

Table S3. Power-law fit parameters for the relationship $N_d = C \cdot S_c^k$ derived from log–log regression. The coefficients C and k are reported as Monte Carlo means ± 1σ (n = 5000 realizations). The coefficient of determination (R^2) and root-mean-square error (RMSE) are calculated from the nominal fit in logarithmic space. Data are filtered using threshold criteria $N_d > N_{d,\mathrm{th}}$ and $\mathrm{LWC} > \mathrm{LWC_{th}}$. The uncertainties of N_d and S_c assumed in the calculations are 10% and 9.5%, respectively. Columns list: Flight ID, $N_{d,\mathrm{th}}$, $\mathrm{LWC_{th}}$, C, σ C, k, σ k, R^2, RMSE, and sample size (N).

Flight	$N_{d,\mathrm{th}}$,	$\mathrm{LWC_{th}}$	C	σC	k	σk	R^2	RMSE	N
AC07	10	0	246.3	3.76	0.894	0.011	0.787	0.639	81
AC07	10	0.01	241.14	4.56	0.917	0.017	0.663	0.672	71
AC07	10	0.02	239.92	6.17	0.923	0.024	0.542	0.691	64
AC07	**20**	**0**	**268.24**	**4.25**	**0.931**	**0.012**	**0.958**	**0.249**	**77**
AC07	20	0.01	263.13	5.02	0.953	0.016	0.948	0.233	69
AC07	20	0.02	265.5	6.41	0.946	0.021	0.942	0.194	62
AC07	30	0	269.41	4.36	0.926	0.012	0.956	0.249	76
AC07	30	0.01	263.13	5.02	0.953	0.016	0.948	0.233	69
AC07	30	0.02	265.5	6.41	0.946	0.021	0.942	0.194	62
AC09	10	0	202.17	4.23	0.837	0.013	0.957	0.243	48
AC09	10	0.01	206.62	4.42	0.82	0.026	0.943	0.166	37
AC09	10	0.02	203.28	4.86	0.865	0.038	0.913	0.17	32
AC09	**20**	**0**	**204.84**	**4.36**	**0.835**	**0.02**	**0.953**	**0.188**	**41**
AC09	20	0.01	206.62	4.42	0.82	0.026	0.943	0.166	37
AC09	20	0.02	203.28	4.86	0.865	0.038	0.913	0.17	32
AC09	30	0	206.21	4.39	0.827	0.025	0.951	0.164	38
AC09	30	0.01	206.62	4.42	0.82	0.026	0.943	0.166	37
AC09	30	0.02	203.28	4.86	0.865	0.038	0.913	0.17	32
AC11	10	0	171.16	4.84	0.951	0.018	0.99	0.121	35
AC11	10	0.01	170.26	6.36	0.955	0.025	0.983	0.12	33
AC11	10	0.02	176.3	7.27	0.933	0.027	0.981	0.114	32
AC11	**20**	**0**	**170.26**	**6.36**	**0.955**	**0.025**	**0.983**	**0.12**	**33**
AC11	20	0.01	170.26	6.36	0.955	0.025	0.983	0.12	33
AC11	20	0.02	176.3	7.27	0.933	0.027	0.981	0.114	32
AC11	30	0	170.26	6.36	0.955	0.025	0.983	0.12	33
AC11	30	0.01	170.26	6.36	0.955	0.025	0.983	0.12	33
AC11	30	0.02	176.3	7.27	0.933	0.027	0.981	0.114	32
AC14	10	0	172.53	3.07	0.968	0.013	0.981	0.174	74
AC14	10	0.01	167.28	3.45	0.998	0.016	0.979	0.158	70
AC14	10	0.02	173.05	4.23	0.972	0.018	0.974	0.147	65
AC14	**20**	**0**	**168.55**	**3.17**	**0.991**	**0.014**	**0.983**	**0.157**	**73**
AC14	20	0.01	167.28	3.45	0.998	0.016	0.979	0.158	70
AC14	20	0.02	173.05	4.23	0.972	0.018	0.974	0.147	65

AC14	30	0	167.31	3.64	0.997	0.016	0.977	0.159	69
AC14	30	0.01	167.31	3.64	0.997	0.016	0.977	0.159	69
AC14	30	0.02	173.05	4.23	0.972	0.018	0.974	0.147	65
AC17a	10	0	171.04	2.16	0.946	0.008	0.964	0.262	131
AC17a	10	0.01	176.01	2.85	0.926	0.012	0.938	0.255	117
AC17a	10	0.02	175.85	3.71	0.927	0.015	0.906	0.259	108
AC17a	**20**	**0**	**175.97**	**2.61**	**0.926**	**0.011**	**0.95**	**0.252**	**121**
AC17a	20	0.01	176.01	2.85	0.926	0.012	0.938	0.255	117
AC17a	20	0.02	175.85	3.71	0.927	0.015	0.906	0.259	108
AC17a	30	0	177.47	2.9	0.919	0.012	0.935	0.254	116
AC17a	30	0.01	177.47	2.9	0.919	0.012	0.935	0.254	116
AC17a	30	0.02	175.85	3.71	0.927	0.015	0.906	0.259	108
AC17b	10	0	213.86	3.88	0.929	0.011	0.979	0.196	69
AC17b	10	0.01	199.07	5.12	0.988	0.018	0.976	0.151	63
AC17b	10	0.02	201.81	5.76	0.979	0.02	0.97	0.152	61
AC17b	**20**	**0**	**202.3**	**4.86**	**0.976**	**0.017**	**0.977**	**0.153**	**64**
AC17b	20	0.01	199.07	5.12	0.988	0.018	0.976	0.151	63
AC17b	20	0.02	201.81	5.76	0.979	0.02	0.97	0.152	61
AC17b	30	0	202.3	4.86	0.976	0.017	0.977	0.153	64
AC17b	30	0.01	199.07	5.12	0.988	0.018	0.976	0.151	63
AC17b	30	0.02	201.81	5.76	0.979	0.02	0.97	0.152	61
AC18	10	0	190.81	2.4	0.877	0.01	0.962	0.21	106
AC18	10	0.01	193.45	2.72	0.857	0.015	0.929	0.209	96
AC18	10	0.02	198.4	3.37	0.824	0.02	0.885	0.208	87
AC18	**20**	**0**	**192.87**	**2.65**	**0.859**	**0.014**	**0.942**	**0.209**	**99**
AC18	20	0.01	193.45	2.72	0.857	0.015	0.929	0.209	96
AC18	20	0.02	198.4	3.37	0.824	0.02	0.885	0.208	87
AC18	30	0	193.45	2.72	0.857	0.015	0.929	0.209	96
AC18	30	0.01	193.45	2.72	0.857	0.015	0.929	0.209	96
AC18	30	0.02	198.4	3.37	0.824	0.02	0.885	0.208	87
AC19	10	0	120.43	1.24	0.868	0.011	0.914	0.245	177
AC19	10	0.01	120.91	1.24	0.85	0.014	0.878	0.242	164
AC19	10	0.02	121.27	1.28	0.835	0.018	0.82	0.241	148
AC19	**20**	**0**	**121.18**	**1.24**	**0.839**	**0.014**	**0.876**	**0.238**	**163**
AC19	20	0.01	121.18	1.24	0.839	0.014	0.876	0.238	163
AC19	20	0.02	121.27	1.28	0.835	0.018	0.82	0.241	148
AC19	30	0	121.6	1.26	0.823	0.016	0.85	0.241	157
AC19	30	0.01	121.6	1.26	0.823	0.016	0.85	0.241	157
AC19	30	0.02	121.27	1.28	0.835	0.018	0.82	0.241	148

Table S4. Power-law fit parameters for the relationship $N_d = C \cdot S_v^k$ derived from log–log regression. The coefficients $C$and $k$are reported as Monte Carlo means ± 1σ (n = 5000 realizations). The coefficient of determination (R^2) and root-mean-square error (RMSE) are calculated from the nominal fit in logarithmic space. Data are filtered using threshold criteria $N_d > N_{d,\mathrm{th}}$ and $\mathrm{LWC} > \mathrm{LWC_{th}}$. The uncertainties of Nd and Sv assumed in the calculations are 30% and 36.6%, respectively. Columns list: Flight ID, $N_{d,\mathrm{th}}$, $\mathrm{LWC_{th}}$, C, σ C, k, σ k, R^2, RMSE, and sample size (N).

Flight	$N_{d,\mathrm{th}}$	$\mathrm{LWC_{th}}$	C	σC	k	σk	R^2	RMSE	N
AC07	10	0	1721.2	192.16	0.802	0.051	0.783	0.645	81
AC07	10	0.01	1646.06	218.54	0.765	0.075	0.657	0.678	71
AC07	10	0.02	1539.65	240.42	0.702	0.098	0.533	0.698	64
AC07	**20**	**0**	**2014.97**	**231.49**	**0.827**	**0.055**	**0.958**	**0.249**	**77**
AC07	20	0.01	1960.94	247.89	0.801	0.073	0.947	0.234	69
AC07	20	0.02	1813.89	252.3	0.731	0.09	0.943	0.193	62
AC07	30	0	1988.67	227.02	0.818	0.055	0.956	0.25	76
AC07	30	0.01	1960.94	247.89	0.801	0.073	0.947	0.234	69
AC07	30	0.02	1813.89	252.3	0.731	0.09	0.943	0.193	62
AC09	10	0	1103.63	193.86	0.758	0.059	0.956	0.244	48
AC09	10	0.01	900.9	217.98	0.642	0.103	0.941	0.169	37
AC09	10	0.02	839.96	246.48	0.593	0.137	0.91	0.173	32
AC09	**20**	**0**	**1006.72**	**213.9**	**0.705**	**0.084**	**0.952**	**0.19**	**41**
AC09	20	0.01	900.9	217.98	0.642	0.103	0.941	0.169	37
AC09	20	0.02	839.96	246.48	0.593	0.137	0.91	0.173	32
AC09	30	0	933.33	218.37	0.662	0.098	0.949	0.167	38
AC09	30	0.01	900.9	217.98	0.642	0.103	0.941	0.169	37
AC09	30	0.02	839.96	246.48	0.593	0.137	0.91	0.173	32
AC11	10	0	1414.52	175.01	0.844	0.075	0.99	0.125	35
AC11	10	0.01	1339.18	180.85	0.785	0.101	0.982	0.125	33
AC11	10	0.02	1294.82	175.18	0.742	0.11	0.98	0.118	32
AC11	**20**	**0**	**1339.18**	**180.85**	**0.785**	**0.101**	**0.982**	**0.125**	**33**
AC11	20	0.01	1339.18	180.85	0.785	0.101	0.982	0.125	33
AC11	20	0.02	1294.82	175.18	0.742	0.11	0.98	0.118	32
AC11	30	0	1339.18	180.85	0.785	0.101	0.982	0.125	33
AC11	30	0.01	1339.18	180.85	0.785	0.101	0.982	0.125	33
AC11	30	0.02	1294.82	175.18	0.742	0.11	0.98	0.118	32
AC14	10	0	1374.34	139.07	0.855	0.056	0.979	0.18	74
AC14	10	0.01	1366.47	152.1	0.844	0.072	0.977	0.166	70
AC14	10	0.02	1294.32	145.45	0.784	0.08	0.972	0.153	65
AC14	**20**	**0**	**1390.5**	**146.66**	**0.862**	**0.061**	**0.981**	**0.164**	**73**
AC14	20	0.01	1366.47	152.1	0.844	0.072	0.977	0.166	70
AC14	20	0.02	1294.32	145.45	0.784	0.08	0.972	0.153	65
AC14	30	0	1355.09	150.79	0.836	0.074	0.975	0.167	69

AC14	30	0.01	1355.09	150.79	0.836	0.074	0.975	0.167	69
AC14	30	0.02	1294.32	145.45	0.784	0.08	0.972	0.153	65
AC17a	10	0	1320.21	95.94	0.849	0.038	0.961	0.271	131
AC17a	10	0.01	1225.93	98.67	0.774	0.054	0.934	0.263	117
AC17a	10	0.02	1168.27	101.36	0.718	0.067	0.9	0.267	108
AC17a	**20**	**0**	**1254.73**	**99.58**	**0.796**	**0.049**	**0.947**	**0.26**	**121**
AC17a	20	0.01	1225.93	98.67	0.774	0.054	0.934	0.263	117
AC17a	20	0.02	1168.27	101.36	0.718	0.067	0.9	0.267	108
AC17a	30	0	1213.02	100.58	0.763	0.055	0.931	0.263	116
AC17a	30	0.01	1213.02	100.58	0.763	0.055	0.931	0.263	116
AC17a	30	0.02	1168.27	101.36	0.718	0.067	0.9	0.267	108
AC17b	10	0	1697.48	157.11	0.841	0.051	0.978	0.201	69
AC17b	10	0.01	1648.07	178.79	0.807	0.079	0.973	0.159	63
AC17b	10	0.02	1600.21	178.1	0.773	0.086	0.967	0.16	61
AC17b	**20**	**0**	**1654.08**	**175.36**	**0.812**	**0.074**	**0.975**	**0.161**	**64**
AC17b	20	0.01	1648.07	178.79	0.807	0.079	0.973	0.159	63
AC17b	20	0.02	1600.21	178.1	0.773	0.086	0.967	0.16	61
AC17b	30	0	1654.08	175.36	0.812	0.074	0.975	0.161	64
AC17b	30	0.01	1648.07	178.79	0.807	0.079	0.973	0.159	63
AC17b	30	0.02	1600.21	178.1	0.773	0.086	0.967	0.16	61
AC18	10	0	1176.15	130.06	0.765	0.048	0.961	0.214	106
AC18	10	0.01	1013.18	134.56	0.676	0.067	0.927	0.212	96
AC18	10	0.02	881.14	130.89	0.582	0.081	0.881	0.211	87
AC18	**20**	**0**	**1063.6**	**131.77**	**0.706**	**0.06**	**0.94**	**0.213**	**99**
AC18	20	0.01	1013.18	134.56	0.676	0.067	0.927	0.212	96
AC18	20	0.02	881.14	130.89	0.582	0.081	0.881	0.211	87
AC18	30	0	1013.18	134.56	0.676	0.067	0.927	0.212	96
AC18	30	0.01	1013.18	134.56	0.676	0.067	0.927	0.212	96
AC18	30	0.02	881.14	130.89	0.582	0.081	0.881	0.211	87
AC19	10	0	534	64.12	0.695	0.05	0.912	0.247	177
AC19	10	0.01	466.78	62.42	0.625	0.059	0.875	0.244	164
AC19	10	0.02	400.16	62.31	0.539	0.072	0.817	0.243	148
AC19	**20**	**0**	**456.91**	**61.43**	**0.614**	**0.059**	**0.874**	**0.24**	**163**
AC19	20	0.01	456.91	61.43	0.614	0.059	0.874	0.24	163
AC19	20	0.02	400.16	62.31	0.539	0.072	0.817	0.243	148
AC19	30	0	425.99	59.82	0.576	0.063	0.847	0.243	157
AC19	30	0.01	425.99	59.82	0.576	0.063	0.847	0.243	157
AC19	30	0.02	400.16	62.31	0.539	0.072	0.817	0.243	148

Table S5. Power-law fit parameters for the relationship $N_d = C \cdot S_l^k$ derived from log–log regression. The coefficients $C$and $k$are reported as Monte Carlo means ± 1σ (n = 5000 realizations). The coefficient of determination (R^2) and root-mean-square error (RMSE) are calculated from the nominal fit in logarithmic space. Data are filtered using threshold criteria $N_d > N_{d,\mathrm{th}}$ and $\mathrm{LWC} > \mathrm{LWC_{th}}$. The uncertainties of N_d and S_l assumed in the calculations are 30% and 27.6%, respectively. Columns list: Flight ID, $N_{d,\mathrm{th}}$, $\mathrm{LWC_{th}}$, C, σ C, k, σ k, R^2, RMSE, and sample size (N).

Flight	$N_{d,\mathrm{th}}$,	$\mathrm{LWC_{th}}$	C	σC	k	σk	R^2	RMSE	N
AC07	10	0	266.51	13.55	0.854	0.039	0.788	0.638	81
AC07	10	0.01	269	16.61	0.848	0.057	0.664	0.671	71
AC07	10	0.02	279.13	22.2	0.817	0.078	0.543	0.691	64
AC07	**20**	**0**	**293.02**	**15.35**	**0.884**	**0.043**	**0.958**	**0.249**	**77**
AC07	20	0.01	294.93	18.34	0.882	0.054	0.948	0.233	69
AC07	20	0.02	309.74	24.01	0.839	0.07	0.942	0.194	62
AC07	30	0	294.72	15.87	0.877	0.042	0.956	0.249	76
AC07	30	0.01	294.93	18.34	0.882	0.054	0.948	0.233	69
AC07	30	0.02	309.74	24.01	0.839	0.07	0.942	0.194	62
AC09	10	0	211.93	14.99	0.802	0.046	0.957	0.243	48
AC09	10	0.01	217.7	15.39	0.731	0.085	0.944	0.166	37
AC09	10	0.02	219.48	16.18	0.717	0.117	0.913	0.169	32
AC09	**20**	**0**	**215.09**	**15.29**	**0.773**	**0.067**	**0.953**	**0.188**	**41**
AC09	20	0.01	217.7	15.39	0.731	0.085	0.944	0.166	37
AC09	20	0.02	219.48	16.18	0.717	0.117	0.913	0.169	32
AC09	30	0	216.99	15.33	0.746	0.081	0.951	0.164	38
AC09	30	0.01	217.7	15.39	0.731	0.085	0.944	0.166	37
AC09	30	0.02	219.48	16.18	0.717	0.117	0.913	0.169	32
AC11	10	0	193.46	18.27	0.907	0.06	0.99	0.121	35
AC11	10	0.01	200.94	24.17	0.88	0.083	0.983	0.12	33
AC11	10	0.02	211.29	27.99	0.847	0.09	0.981	0.114	32
AC11	**20**	**0**	**200.94**	**24.17**	**0.88**	**0.083**	**0.983**	**0.12**	**33**
AC11	20	0.01	200.94	24.17	0.88	0.083	0.983	0.12	33
AC11	20	0.02	211.29	27.99	0.847	0.09	0.981	0.114	32
AC11	30	0	200.94	24.17	0.88	0.083	0.983	0.12	33
AC11	30	0.01	200.94	24.17	0.88	0.083	0.983	0.12	33
AC11	30	0.02	211.29	27.99	0.847	0.09	0.981	0.114	32
AC14	10	0	193.24	11.46	0.919	0.043	0.981	0.173	74
AC14	10	0.01	192.2	13.05	0.929	0.053	0.979	0.157	70
AC14	10	0.02	203.97	16.47	0.883	0.062	0.974	0.147	65
AC14	**20**	**0**	**190.74**	**11.89**	**0.935**	**0.047**	**0.983**	**0.157**	**73**
AC14	20	0.01	192.2	13.05	0.929	0.053	0.979	0.157	70
AC14	20	0.02	203.97	16.47	0.883	0.062	0.974	0.147	65
AC14	30	0	193.31	13.75	0.925	0.056	0.977	0.158	69
AC14	30	0.01	193.31	13.75	0.925	0.056	0.977	0.158	69

AC14	30	0.02	203.97	16.47	0.883	0.062	0.974	0.147	65
AC17a	10	0	189.08	7.94	0.909	0.029	0.964	0.261	131
AC17a	10	0.01	200.53	10.66	0.862	0.04	0.938	0.254	117
AC17a	10	0.02	208.84	14.3	0.831	0.052	0.907	0.258	108
AC17a	**20**	**0**	**198.01**	**9.81**	**0.872**	**0.037**	**0.951**	**0.251**	**121**
AC17a	20	0.01	200.53	10.66	0.862	0.04	0.938	0.254	117
AC17a	20	0.02	208.84	14.3	0.831	0.052	0.907	0.258	108
AC17a	30	0	202.61	10.9	0.853	0.042	0.935	0.254	116
AC17a	30	0.01	202.61	10.9	0.853	0.042	0.935	0.254	116
AC17a	30	0.02	208.84	14.3	0.831	0.052	0.907	0.258	108
AC17b	10	0	236.59	14.36	0.893	0.039	0.979	0.195	69
AC17b	10	0.01	234.73	19.91	0.906	0.061	0.976	0.15	63
AC17b	10	0.02	242.52	22.71	0.883	0.068	0.97	0.151	61
AC17b	**20**	**0**	**235.49**	**18.71**	**0.903**	**0.057**	**0.977**	**0.153**	**64**
AC17b	20	0.01	234.73	19.91	0.906	0.061	0.976	0.15	63
AC17b	20	0.02	242.52	22.71	0.883	0.068	0.97	0.151	61
AC17b	30	0	235.49	18.71	0.903	0.057	0.977	0.153	64
AC17b	30	0.01	234.73	19.91	0.906	0.061	0.976	0.15	63
AC17b	30	0.02	242.52	22.71	0.883	0.068	0.97	0.151	61
AC18	10	0	204.42	8.54	0.827	0.036	0.962	0.21	106
AC18	10	0.01	210.96	9.57	0.77	0.051	0.93	0.208	96
AC18	10	0.02	221.76	11.57	0.699	0.066	0.885	0.207	87
AC18	**20**	**0**	**208.54**	**9.32**	**0.787**	**0.047**	**0.942**	**0.209**	**99**
AC18	20	0.01	210.96	9.57	0.77	0.051	0.93	0.208	96
AC18	20	0.02	221.76	11.57	0.699	0.066	0.885	0.207	87
AC18	30	0	210.96	9.57	0.77	0.051	0.93	0.208	96
AC18	30	0.01	210.96	9.57	0.77	0.051	0.93	0.208	96
AC18	30	0.02	221.76	11.57	0.699	0.066	0.885	0.207	87
AC19	10	0	126.59	4.38	0.784	0.038	0.914	0.244	177
AC19	10	0.01	127.24	4.34	0.736	0.046	0.878	0.241	164
AC19	10	0.02	128.75	4.35	0.674	0.059	0.82	0.241	148
AC19	**20**	**0**	**127.43**	**4.34**	**0.724**	**0.047**	**0.876**	**0.238**	**163**
AC19	20	0.01	127.43	4.34	0.724	0.047	0.876	0.238	163
AC19	20	0.02	128.75	4.35	0.674	0.059	0.82	0.241	148
AC19	30	0	127.99	4.32	0.693	0.051	0.85	0.24	157
AC19	30	0.01	127.99	4.32	0.693	0.051	0.85	0.24	157
AC19	30	0.02	128.75	4.35	0.674	0.059	0.82	0.241	148

Table S6. Power-law fit parameters for the relationship $N_d = C \cdot S_c^k$ derived from log–log regression. The coefficients C and k are reported as Monte Carlo means ± 1σ (n = 5000 realizations). The coefficient of determination (R^2) and root-mean-square error (RMSE) are calculated from the nominal fit in logarithmic space. Data are filtered using threshold criteria $N_d > N_{d,\mathrm{th}}$ and $\mathrm{LWC} > \mathrm{LWC_{th}}$. The uncertainties of N_d and S_c assumed in the calculations are 30% and 28.5%, respectively. Columns list: Flight ID, $N_{d,\mathrm{th}}$, $\mathrm{LWC_{th}}$, C, σ C, k, σ k, R^2, RMSE, and sample size (N).

Flight	$N_{d,\mathrm{th}}$,	$\mathrm{LWC_{th}}$	C	σC	k	σk	R^2	RMSE	N
AC07	10	0	246.01	12.94	0.85	0.04	0.787	0.639	81
AC07	10	0.01	249.2	16.59	0.841	0.058	0.663	0.672	71
AC07	10	0.02	260.33	22.76	0.807	0.081	0.542	0.691	64
AC07	**20**	**0**	**269.85**	**14.76**	**0.879**	**0.044**	**0.958**	**0.249**	**77**
AC07	20	0.01	272.28	18.1	0.875	0.056	0.948	0.233	69
AC07	20	0.02	288.17	24.58	0.83	0.072	0.942	0.194	62
AC07	30	0	271.65	15.23	0.872	0.044	0.956	0.249	76
AC07	30	0.01	272.28	18.1	0.875	0.056	0.948	0.233	69
AC07	30	0.02	288.17	24.58	0.83	0.072	0.942	0.194	62
AC09	10	0	194.3	13.42	0.798	0.047	0.957	0.243	48
AC09	10	0.01	201.34	14.07	0.723	0.087	0.943	0.166	37
AC09	10	0.02	203.71	15.63	0.706	0.12	0.913	0.17	32
AC09	**20**	**0**	**197.88**	**13.73**	**0.767**	**0.068**	**0.953**	**0.188**	**41**
AC09	20	0.01	201.34	14.07	0.723	0.087	0.943	0.166	37
AC09	20	0.02	203.71	15.63	0.706	0.12	0.913	0.17	32
AC09	30	0	200.33	13.94	0.739	0.082	0.951	0.164	38
AC09	30	0.01	201.34	14.07	0.723	0.087	0.943	0.166	37
AC09	30	0.02	203.71	15.63	0.706	0.12	0.913	0.17	32
AC11	10	0	178.21	18.02	0.901	0.061	0.99	0.121	35
AC11	10	0.01	186.53	24.5	0.871	0.085	0.983	0.12	33
AC11	10	0.02	197.14	28.73	0.837	0.092	0.981	0.114	32
AC11	**20**	**0**	**186.53**	**24.5**	**0.871**	**0.085**	**0.983**	**0.12**	**33**
AC11	20	0.01	186.53	24.5	0.871	0.085	0.983	0.12	33
AC11	20	0.02	197.14	28.73	0.837	0.092	0.981	0.114	32
AC11	30	0	186.53	24.5	0.871	0.085	0.983	0.12	33
AC11	30	0.01	186.53	24.5	0.871	0.085	0.983	0.12	33
AC11	30	0.02	197.14	28.73	0.837	0.092	0.981	0.114	32
AC14	10	0	176.81	11.14	0.914	0.045	0.981	0.174	74
AC14	10	0.01	176.04	12.88	0.922	0.055	0.979	0.158	70
AC14	10	0.02	188.13	16.62	0.875	0.064	0.974	0.147	65
AC14	**20**	**0**	**174.38**	**11.65**	**0.929**	**0.049**	**0.983**	**0.157**	**73**
AC14	20	0.01	176.04	12.88	0.922	0.055	0.979	0.158	70
AC14	20	0.02	188.13	16.62	0.875	0.064	0.974	0.147	65
AC14	30	0	177.23	13.63	0.917	0.057	0.977	0.159	69
AC14	30	0.01	177.23	13.63	0.917	0.057	0.977	0.159	69

AC14	30	0.02	188.13	16.62	0.875	0.064	0.974	0.147	65
AC17a	10	0	173.11	7.66	0.903	0.03	0.964	0.262	131
AC17a	10	0.01	185.21	10.82	0.853	0.043	0.938	0.255	117
AC17a	10	0.02	194.26	14.82	0.821	0.055	0.906	0.259	108
AC17a	**20**	**0**	**182.36**	**9.74**	**0.865**	**0.038**	**0.95**	**0.252**	**121**
AC17a	20	0.01	185.21	10.82	0.853	0.043	0.938	0.255	117
AC17a	20	0.02	194.26	14.82	0.821	0.055	0.906	0.259	108
AC17a	30	0	187.33	11.03	0.845	0.044	0.935	0.254	116
AC17a	30	0.01	187.33	11.03	0.845	0.044	0.935	0.254	116
AC17a	30	0.02	194.26	14.82	0.821	0.055	0.906	0.259	108
AC17b	10	0	217.89	13.9	0.889	0.04	0.979	0.196	69
AC17b	10	0.01	217.1	20.02	0.898	0.063	0.976	0.151	63
AC17b	10	0.02	225.27	23.23	0.873	0.07	0.97	0.152	61
AC17b	**20**	**0**	**217.62**	**18.73**	**0.895**	**0.059**	**0.977**	**0.153**	**64**
AC17b	20	0.01	217.1	20.02	0.898	0.063	0.976	0.151	63
AC17b	20	0.02	225.27	23.23	0.873	0.07	0.97	0.152	61
AC17b	30	0	217.62	18.73	0.895	0.059	0.977	0.153	64
AC17b	30	0.01	217.1	20.02	0.898	0.063	0.976	0.151	63
AC17b	30	0.02	225.27	23.23	0.873	0.07	0.97	0.152	61
AC18	10	0	188.64	8	0.822	0.037	0.962	0.21	106
AC18	10	0.01	196.19	9.42	0.762	0.053	0.929	0.209	96
AC18	10	0.02	208.19	11.92	0.688	0.068	0.885	0.208	87
AC18	**20**	**0**	**193.44**	**9.02**	**0.781**	**0.048**	**0.942**	**0.209**	**99**
AC18	20	0.01	196.19	9.42	0.762	0.053	0.929	0.209	96
AC18	20	0.02	208.19	11.92	0.688	0.068	0.885	0.208	87
AC18	30	0	196.19	9.42	0.762	0.053	0.929	0.209	96
AC18	30	0.01	196.19	9.42	0.762	0.053	0.929	0.209	96
AC18	30	0.02	208.19	11.92	0.688	0.068	0.885	0.208	87
AC19	10	0	115.44	3.86	0.777	0.039	0.914	0.245	177
AC19	10	0.01	116.76	3.86	0.726	0.048	0.878	0.242	164
AC19	10	0.02	119.15	4.02	0.661	0.061	0.82	0.241	148
AC19	**20**	**0**	**117.09**	**3.86**	**0.715**	**0.048**	**0.876**	**0.238**	**163**
AC19	20	0.01	117.09	3.86	0.715	0.048	0.876	0.238	163
AC19	20	0.02	119.15	4.02	0.661	0.061	0.82	0.241	148
AC19	30	0	118.08	3.91	0.683	0.052	0.85	0.241	157
AC19	30	0.01	118.08	3.91	0.683	0.052	0.85	0.241	157
AC19	30	0.02	119.15	4.02	0.661	0.061	0.82	0.241	148